Chapter 12

Flavor physics

Quarks and leptons can be ordered in flavour doublets, each column being called a family,

$$\begin{array}{lcccc} \text{Quarks:} & \begin{pmatrix} u \\ d \end{pmatrix} & \begin{pmatrix} c \\ s \end{pmatrix} & \begin{pmatrix} t \\ b \end{pmatrix} & \begin{array}{c} Q = \frac{2}{3} \\ Q = -\frac{1}{3} \end{array} , \\ \text{Leptons:} & \begin{pmatrix} \nu_e \\ e \end{pmatrix} & \begin{pmatrix} \nu_\mu \\ \mu \end{pmatrix} & \begin{pmatrix} \nu_\tau \\ \tau \end{pmatrix} & \begin{array}{c} Q = 0 \\ Q = -1 \end{array} . \end{array}$$

These arrangements correspond to an approximate flavor $SU(6)$ symmetry. The isospin $SU(2)$ of p, n (Sect. 7, p. 125) or the flavor $SU(3)$ symmetry of u, d, s (Sect. 7.3, p. 131) are much better fulfilled since the mass differences between the different particles are much smaller than the masses themselves.

12.1 Cabibbo angle

The structure of the charged currents,

$$j_\mu^\pm = \bar{\chi}_L \gamma_\mu \tau_\pm \chi_L,$$

allows transitions within a single doublet, e.g. $d \to u$, $c \to s$, $t \to b$, but not between different doublets. This would imply that the lightest particle of each doublet should be stable (the electromagnetic and strong interactions do not allow flavor changing processes, since photons and gluons do not carry any flavor quantum numbers), a fact which is in contradiction with the observation that our universe is composed almost exclusively of particles of the first family, consisting of the lightest particles.

Assuming that the weak eigenstates of the d-type quarks [1] are linear combinations of the mass eigenstates one can reproduce the observed phenomenology. Let us first consider the

[1] Some authors prefer to rotate the u-type quarks. We follow here the most common version.

case of two quark families for simplicity. We have the weak eigenstate doublets,

$$\begin{pmatrix} u \\ d' \end{pmatrix} \quad \begin{pmatrix} c \\ s' \end{pmatrix},$$

and we assume that the weak eigenstates $|d'\rangle$ and $|s'\rangle$ are linear combinations of the mass eigenstates $|d\rangle$ and $|s\rangle$,

$$\begin{aligned} |d'\rangle &= \cos\theta_c\,|d\rangle + \sin\theta_c\,|s\rangle \\ |s'\rangle &= -\sin\theta_c\,|d\rangle + \cos\theta_c\,|s\rangle\,, \end{aligned} \tag{12.1}$$

where θ_c is called the **Cabibbo angle**.

Since decaying particles and decay products are mass eigenstates, this trick allows transitions between different families. Using Eq. (12.1), we can write vertex factors between mass eigenstates,

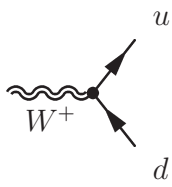

$\propto \cos\theta_c$

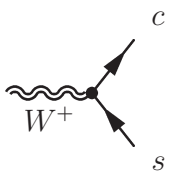

$\propto \cos\theta_c,$

called **Cabibbo preferred decays**, and,

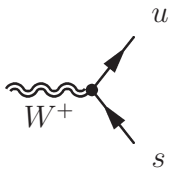

$\propto \sin\theta_c$

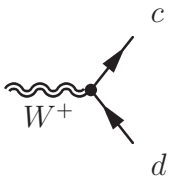

$\propto -\sin\theta_c,$

called **Cabibbo suppressed decays**. If the weak and mass eigenstates would be the same, $\theta_c = 0$ and the second series of decay could not occur. The kaons are unstable but have a relatively long lifetime, since the decay of the s quark is Cabibbo supressed.

The introduction of the Cabibbo angle also destroys the universality of the Fermi constant,

$$G_F^{n\to pe^-\bar{\nu}_e} = \cos\theta_c G_F^{\mu^-\to e^-\nu_\mu\bar{\nu}_e}, \tag{12.2}$$

with the experimentally measured value,

$$\cos\theta_c \approx 0.974. \tag{12.3}$$

We can now rewrite the interaction Lagrangian for the charged current coupling to quarks,

$$\begin{aligned} i\mathcal{L}_{int}^{W^{\pm},q} = &- i\frac{g}{\sqrt{2}} \begin{pmatrix} \bar{u} & \bar{c} \end{pmatrix} \gamma_\mu \frac{1-\gamma_5}{2} U \begin{pmatrix} d \\ s \end{pmatrix} W^{+\mu} \\ &- i\frac{g}{\sqrt{2}} \begin{pmatrix} \bar{d} & \bar{s} \end{pmatrix} U^T \gamma_\mu \frac{1-\gamma_5}{2} \begin{pmatrix} u \\ c \end{pmatrix} W^{-\mu}, \end{aligned} \tag{12.4}$$

with,

$$U = \begin{pmatrix} \cos\theta_c & \sin\theta_c \\ -\sin\theta_c & \cos\theta_c \end{pmatrix} \in U(2). \tag{12.5}$$

We remark at this point, that $U = U^*$ or in other words $U \in O(2)$ implying that $U^\dagger = U^T$.

12.2 Cabibbo-Kobayashi-Maskawa matrix

In 1973, before the observation of c, b and t quarks, the existence of three families and its implications were already hypothesised.

Analogously to Eq. (12.4), we write for three families,

$$\begin{aligned} i\mathcal{L}_{int}^{W^{\pm},q} = &- i\frac{g}{\sqrt{2}} \begin{pmatrix} \bar{u} & \bar{c} & \bar{t} \end{pmatrix} \gamma_\mu \frac{1-\gamma_5}{2} V \begin{pmatrix} d \\ s \\ b \end{pmatrix} W^{+\mu} \\ &- i\frac{g}{\sqrt{2}} \begin{pmatrix} \bar{d} & \bar{s} & \bar{b} \end{pmatrix} V^\dagger \gamma_\mu \frac{1-\gamma_5}{2} \begin{pmatrix} u \\ c \\ t \end{pmatrix} W^{-\mu}, \end{aligned} \tag{12.6}$$

where $V \in U(3)$.

Recall that for a matrix $V \in U(N)$:

- V contains N^2 real parameters ($2N^2$ entries minus N^2 from the unitarity condition $V^\dagger V = \mathbb{1}$),
- $2N - 1$ relative phases can be factorized by a phase redefinition of the quantum fields.

Thus V contains $N^2 - (2N-1) = (N-1)^2$ independent real parameters. On the other hand, a matrix $O \in O(N)$ is determined by $\frac{1}{2}N(N-1)$ independent real parameters (Euler angles).

Comparing V and O, we have, $N_a = \frac{1}{2}N(N-1)$ real angles and $N_p = (N-1)^2 - N_a = \frac{1}{2}(N-1)(N-2)$ complex phases. It then easy to see that we always have complex phases for $N \geq 3$, implying $V^* \neq V$.

Looking at the vertex factors connected through a CP-transformation,

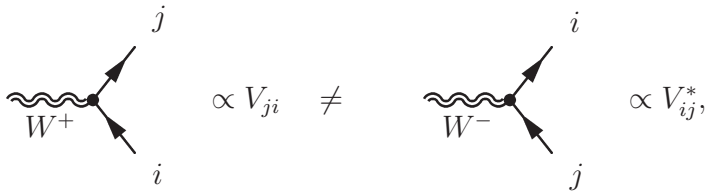

we conclude that the weak interaction violates CP invariance for $N \geq 3$ through complex phases in the CKM matrix V.

12.3 Neutrino mixing

Literature:

- Fukugita/Yanagida [20]

As in the case of d-type quarks, one can consider the phenomenology implied by neutrinos whose mass eigenstates (ν_1, ν_2 and ν_3) are not the same as the weak eigenstates (ν_e, ν_μ and ν_τ). The interaction Lagrangian becomes,

$$\begin{aligned} i\mathcal{L}_{int}^{W^\pm,l} = &- i\frac{g}{\sqrt{2}} \begin{pmatrix} \bar{\nu}_1 & \bar{\nu}_2 & \bar{\nu}_3 \end{pmatrix} U^\dagger \gamma_\mu \frac{1-\gamma_5}{2} \begin{pmatrix} e \\ \mu \\ \tau \end{pmatrix} W^{+\mu} \\ &- i\frac{g}{\sqrt{2}} \begin{pmatrix} \bar{e} & \bar{\mu} & \bar{\tau} \end{pmatrix} \gamma_\mu \frac{1-\gamma_5}{2} U \begin{pmatrix} \nu_1 \\ \nu_2 \\ \nu_3 \end{pmatrix} W^{-\mu}, \end{aligned} \tag{12.7}$$

with U the unitary neutrino mixing matrix, also called **Pontecorvo-Maki-Nakagawa-Sakata (PMNS) matrix**. As in the case of quarks, the existence of three neutrino families would let room for a CP violation in the neutrino sector . Up to now, it has not been possible to observe it experimentally.

In order to treat neutrino oscillations, it is important to remember the following facts about neutrinos:

- They are always produced as eigenstates of the weak interaction, e.g. $\pi^- \to \mu^- \bar{\nu}_\mu$,
- They are always detected as eigenstates of the weak interaction, e.g. $\nu_\mu p \to \mu^- X$,
- But they propagate in the vacuum as mass eigenstates.

Assuming two lepton families (e, μ), we write the weak eigenstates as,

$$\begin{aligned} |\nu_e\rangle &= \cos\theta\,|\nu_1\rangle + \sin\theta\,|\nu_2\rangle \\ |\nu_\mu\rangle &= -\sin\theta\,|\nu_1\rangle + \cos\theta\,|\nu_2\rangle\,. \end{aligned} \tag{12.8}$$

The time evolution of the mass eigenstates is given by,

$$|\nu_i, t\rangle = \mathrm{e}^{-iE_i t}\,|\nu_i, 0\rangle\,, \tag{12.9}$$

such that the evolution of the weak eigenstates is given by,

$$|\nu_\alpha, t\rangle = \sum_i U_{\alpha i}\mathrm{e}^{-iE_i t}\,|\nu_i, 0\rangle\,. \tag{12.10}$$

Since we know experimentally that $m_{\nu_i} < \mathrm{eV}, \mathrm{keV} \ll E \approx \mathrm{MeV}$, we can safely assume that they are ultrarelativistic and make the approximation,

$$E_i = \sqrt{\vec{p}^{\,2} + m_i^2} \approx |\vec{p}| + \frac{m_i^2}{2|\vec{p}|} = |\vec{p}| + \frac{m_i^2}{2E} \qquad (|\vec{p}| \gg m_i) \tag{12.11}$$

Inserting this in Eq. (12.9) we get,

$$\begin{aligned} |\nu_\alpha, t\rangle &= \mathrm{e}^{-i|\vec{p}|t}\left(U\begin{bmatrix} \mathrm{e}^{-i\frac{m_1^2 t}{2E}} & 0 \\ 0 & \mathrm{e}^{-i\frac{m_2^2 t}{2E}} \end{bmatrix} U^\dagger\right)_{\alpha\beta} |\nu_\beta, t\rangle \\ &\approx \mathrm{e}^{-i|\vec{p}|t}\left(U\begin{bmatrix} 1-\frac{im_1^2 t}{2E} & 0 \\ 0 & 1-\frac{im_2^2 t}{2E} \end{bmatrix} U^\dagger\right)_{\alpha\beta} |\nu_\beta, t\rangle\,, \end{aligned}$$

and, using,

$$U^\dagger m^\dagger m U = m^2_{Diag} = \begin{pmatrix} m_1^2 & 0 \\ 0 & m_2^2 \end{pmatrix},$$

we obtain (reexpressing $1 + iX = \mathrm{e}^{iX}$),

$$|\nu_\alpha, t\rangle = \mathrm{e}^{-i|\vec{p}|t}\left(\mathrm{e}^{-i\frac{m^\dagger m}{2E}t}\right)_{\alpha\beta} |\nu_\beta, 0\rangle\,. \tag{12.12}$$

We can interpret Eq. (12.12) as the solution of the Schrödinger equation,

$$i\frac{d}{dt}\,|\nu_\alpha, t\rangle = \left(|\vec{p}|\delta_{\alpha\beta} + \frac{(m^\dagger m)_{\alpha\beta}}{2E}\right)|\nu_\beta, t\rangle\,. \tag{12.13}$$

We now compute the $m^\dagger m$ matrix,

$$m^\dagger m = U m^2_{Diag} U^\dagger = \begin{pmatrix} m_1^2\cos^2\theta + m_2\sin^2\theta & \frac{1}{2}(m_2^2-m_1^2)\sin 2\theta \\ \frac{1}{2}(m_2^2-m_1^2)\sin 2\theta & m_1^2\sin^2\theta + m_2^2\cos^2\theta \end{pmatrix}$$
$$= \frac{m_1^2+m_2^2}{2}\mathbb{1} + \frac{\Delta m^2}{2}\begin{pmatrix} -\cos 2\theta & \sin 2\theta \\ \sin 2\theta & \cos 2\theta \end{pmatrix},$$

with $\Delta m^2 = m_2^2 - m_1^2$. The term proportional to the identity does not induce a mixing and corresponds to a trivial phase factor. Inserting this result in Eq. (12.13) and dropping the diagonal term, we get,

$$i\frac{d}{dt}\begin{pmatrix} |\nu_e,t\rangle \\ |\nu_\mu,t\rangle \end{pmatrix} = \frac{\Delta m^2}{4E}\begin{pmatrix} -\cos 2\theta & \sin 2\theta \\ \sin 2\theta & \cos 2\theta \end{pmatrix}\begin{pmatrix} |\nu_e,t\rangle \\ |\nu_\mu,t\rangle \end{pmatrix}$$
$$= H_{vac}\begin{pmatrix} |\nu_e,t\rangle \\ |\nu_\mu,t\rangle \end{pmatrix},$$

with solution,

$$\begin{pmatrix} |\nu_e,t\rangle \\ |\nu_\mu,t\rangle \end{pmatrix} = \mathrm{e}^{-iH_{vac}t}\begin{pmatrix} |\nu_e,0\rangle \\ |\nu_\mu,0\rangle \end{pmatrix}.$$

Writing,

$$\mathrm{e}^{-iH_{vac}t} = \begin{pmatrix} A_{ee}(t) & A_{e\mu}(t) \\ A_{\mu e}(t) & A_{\mu\mu}(t) \end{pmatrix},$$

and using,

$$H_{vac} = \frac{\Delta m^2}{2E}\left(\sin(2\theta)\sigma_1 - \cos(2\theta)\sigma_3\right),$$

we get,

$$\mathrm{e}^{-iH_{vac}t} = \cos\left(\frac{\Delta m^2}{2E}t\right)\mathbb{1} - i\sin\left(\frac{\Delta m^2}{2E}t\right)\left(\sin(2\theta)\sigma_1 + \cos(2\theta)\sigma_3\right). \tag{12.14}$$

We finally get the transition amplitude from the projection of $|\nu_e,t\rangle$ onto $\langle\nu_e|$:

$$\langle\nu_e|\nu_e,t\rangle = A_{ee}(t) = \cos\left(\frac{\Delta m^2}{2E}t\right) - i\sin\left(\frac{\Delta m^2}{2E}t\right)\cos 2\theta,$$

and the transition probability,

$$P_{\nu_e\to\nu_e}(t) = |\langle\nu_e|\nu_e,t\rangle|^2 = 1 - \sin^2(2\theta)\sin^2\left(\frac{\Delta m^2}{2E}t\right) \tag{12.15}$$

$$P_{\nu_e\to\nu_\mu}(t) = |\langle\nu_\mu|\nu_e,t\rangle|^2 = \sin^2(2\theta)\sin^2\left(\frac{\Delta m^2}{2E}t\right) \tag{12.16}$$

A useful formula to estimate the distance over which full oscillations take place is (since the neutrino is ultrarelativistic $L = t$),

$$\frac{\Delta m^2 L}{4E} \approx 1.27\frac{\Delta m^2[\mathrm{eV}^2]L[\mathrm{m}]}{E[\mathrm{MeV}]}. \tag{12.17}$$

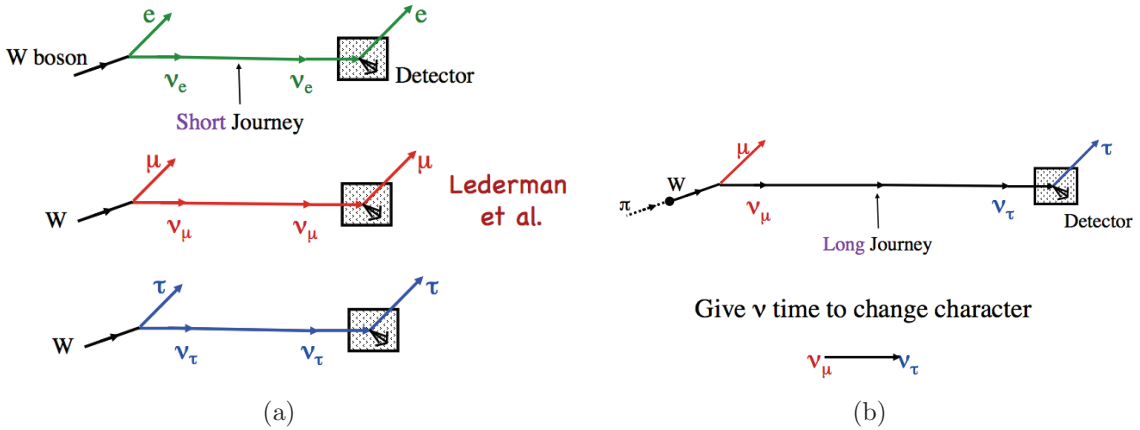

(a) (b)

Figure 12.1: *Neutrino production and detection.* During a sufficiently long journey, the neutrinos may change character (b). Source: B. Kayser.

12.4 Neutrino physics

In the previous sections we have seen that neutrino oscillation can be accounted for by assuming that neutrino flavor eigenstates are not identical to the mass eigenstates. Here we will again take a look at the two-neutrino case, discuss what can be measured in experiment and extend the theoretical treatment of oscillation to the three-neutrino case. Based on these results, we will proceed to the discussion of phenomenological aspects. It will become clear that to measure absolute neutrino masses, different experiments than the ones documenting neutrino oscillations are necessary. Their discussion will conclude this section.[2]

12.4.1 Neutrino oscillation theory revisited

Consider the charged-current interaction or W boson decay $W \to e\nu_e$ (see Fig. 12.1(a)). Since the electron (positron) produced together with its anti-neutrino (neutrino) can be detected and identified, the neutrino flavor at the time of production is fixed and in principle known (see also [24]). Detection of the neutrino proceeds via the inverse process, by lepton number conservation producing again an electron (positron), if the flavor is conserved while the neutrino travels from its place of production to the detector. The analogue holds for μ and τ.

However, if neutrinos have mass, it is possible for them to change their flavor, given the journey to the detector is long enough (see Fig. 12.1(b)). As we have seen, a difference in the mass eigenvalues $\delta m \neq 0$ is a necessary condition for oscillation to occur. Recently, a first candidate for a direct observation of the flavor change $\nu_\mu \to \nu_\tau$ was reported.[3]

[2] This section is heavily based on lectures by E. Lisi at the CHIPP PhD school, Jan. 2010 [21, 22, 23].
[3] `http://operaweb.lngs.infn.it/IMG/pdf/OPERA_press_release_May_2010_english-5.pdf`

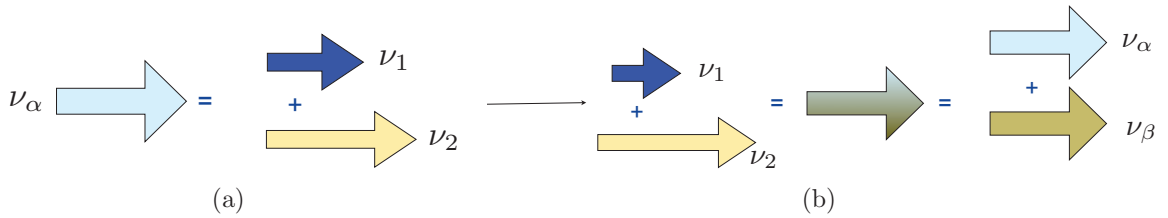

Figure 12.2: *Neutrino mixing in the two-neutrino case.*

In Sect. 12.4.2 we will discuss further experimental evidence that such flavor oscillations actually occur. This means that neutrino flavor is not a constant of motion. From electroweak theory we know that left-handed neutrinos ν_l are produced together with the corresponding lepton l in charged-current interactions (see Sect. 11.5). Recall that the right-handed neutrino carries neither $SU(2)_L$ nor $U(1)_Y$ charge and thus decouples from the electroweak interactions. Recent experiments, probing probabilities $P(\nu_\alpha \to \nu_\beta)$, have found that flavor is not conserved over macroscopic distances, especially in the so-called disappearance mode:

$$P(\nu_e \to \nu_e) < 1$$
$$P(\nu_\mu \to \nu_\mu) < 1$$

means that one finds less events than expected from the production rate, i. e. individual lepton number is not conserved.

These phenomena can be explained by neutrino mixing: For neutrinos, flavor eigenstates $\{\nu_\alpha\}$ are not identical to mass eigenstates $\{\nu_i\}$ and thus they can be expressed as linear combinations of each other. For the left-handed fields this reads, in analogy to the CKM matrix,

$$\nu_{\alpha L} = \sum_{i=1}^{3} U_{\alpha i} \nu_{iL} \tag{12.18}$$

for $\alpha = e, \mu, \tau$. Here $U = U^\dagger$ is called PMNS (Pontecorvo-Maki-Nakagawa-Sakata) matrix with $U \to U^*$ for $\nu \to \bar{\nu}$.

So, how does this setup bring about neutrino mixing? At production we start out with a pure flavor eigenstate ν_α which is according to Eq. (12.18) a certain superposition of mass eigenstates, say ν_1 and ν_2 (see Fig. 12.2(a)). If the eigenvalues of the mass eigenstates are different, so are their energies: $E_1 \neq E_2$. Thus the free time evolution operator introduces different phases and the superposition changes while traveling the distance $L \simeq ct$. Now, neutrino detection is a projection to one *flavor* eigenstate, such that, depending on the mixing angle θ and the mass difference δm^2, the number of produced neutrinos of flavor α may differ from the number of detected neutrinos of this flavor (see Fig. 12.2(b)). Recall that for the two-neutrino case the superpositions can be written as

$$\begin{pmatrix} \nu_\alpha \\ \nu_\beta \end{pmatrix} = \begin{pmatrix} \cos\theta & \sin\theta \\ -\sin\theta & \cos\theta \end{pmatrix} \begin{pmatrix} \nu_1 \\ \nu_2 \end{pmatrix}$$

where θ is the mixing angle. This ansatz predicts the phenomena of "disappearance",

$$P(\nu_\alpha \to \nu_\alpha) = P(\nu_\beta \to \nu_\beta) = P(\bar{\nu}_\alpha \to \bar{\nu}_\alpha) = P(\bar{\nu}_\beta \to \bar{\nu}_\beta) = 1 - \sin^2 2\theta \sin^2 \frac{\Delta_{12}}{2},$$

and "appearance",

$$P(\nu_\alpha \to \nu_\beta) = P(\nu_\beta \to \nu_\alpha) = P(\bar{\nu}_\alpha \to \bar{\nu}_\beta) = P(\bar{\nu}_\beta \to \bar{\nu}_\alpha) = \sin^2 2\theta \sin^2 \frac{\Delta_{12}}{2}$$

where $\Delta_{12} \equiv \Delta m^2 t/(2E) \simeq \Delta m^2 L/(2E)$. Stating the above in another way, we can say that in the two-neutrino case the transition probability is

$$P(\nu_\alpha \to \nu_\beta) = \sin^2 2\theta \sin^2 \frac{\Delta m^2 L}{4E}$$

where

$$\frac{\Delta m^2 L}{4E} = 1.27 \left(\frac{\Delta m^2}{\mathrm{eV}^2}\right) \left(\frac{L}{\mathrm{km}}\right) \left(\frac{\mathrm{GeV}}{E}\right).$$

Let us define the oscillation wavelength

$$\lambda_{\mathrm{osc}} = \frac{4\pi E}{\Delta m^2}$$

and rewrite the transition probability accordingly:

$$P(\nu_\alpha \to \nu_\beta) = \underbrace{\sin^2(2\theta)}_{\text{mixing term}} \underbrace{\sin^2\left(\pi \frac{L}{\lambda_{\mathrm{osc}}}\right)}_{\text{oscillation term}}. \tag{12.19}$$

The LHS of Eq. (12.19) is determined in experiment by counting events and normalizing. Since the mixing angle θ is fixed, so is the mixing term on the RHS. However the oscillation term can be influenced by the experimental design: Although Δm^2 is fixed, the experimenter is free to choose the source-detector distance L and can, by selecting the production process, influence the neutrino energy E and thus λ_{osc}. We now discuss the behavior of Eq. (12.19) for different sizes of L/λ_{osc}.

A) $L/\lambda_{\mathrm{osc}} \ll 1$. E. g. this is realized for $\Delta m^2 \sim 10^{-5}\,\mathrm{eV}^2$ and $E \sim 1\,\mathrm{MeV}$ which is the energy scale of nuclear reactions; at the same time L needs to be small, e. g. $L \sim 1\,\mathrm{km}$. Since the argument of the oscillation term is small, it can be approximated by the first term of the Taylor series:

$$\sin^2\left(\pi \frac{L}{\lambda_{\mathrm{osc}}}\right) \simeq \left(\pi \frac{L}{\lambda_{\mathrm{osc}}}\right)^2.$$

Therefore the transition probability is small and the effect might be very difficult to measure, depending on the experimental resolution.

B) $\pi L/\lambda_{\text{osc}} \simeq 1$. E. g. consider the case that L and E are such that $\pi L/\lambda_{\text{osc}} \simeq \pi/2$, i. e. the oscillation term is at its first maximum. Possible numbers are: $\Delta m^2 \simeq 10^{-3}\,\text{eV}^2$, $E = 1\,\text{GeV}$ (energy scale of accelerators and cosmic rays) and $L \simeq 1000\,\text{km}$. In this case

$$1.27\Delta m^2 \frac{L}{E} \simeq 1.3 \simeq \frac{\pi}{2}$$

such that the sensitivity to the mixing term is maximized.

C) $L/\lambda_{\text{osc}} \gg 1$: For instance, this is the case if $\Delta m^2 \simeq 10^{-5}\,\text{eV}^2$, $L =$ distance earth-sun $\sim 150 \cdot 10^6\,\text{km}$, $E \sim 1\,\text{MeV}$. Therefore, fast oscillation is taking place which leads to a measurement of the average due to uncertainties in E and L:

$$\left\langle \sin^2\left(\pi \frac{L}{\lambda_{\text{osc}}}\right)\right\rangle = \frac{1}{2} \Rightarrow P(\nu_\alpha \to \nu_\beta) = \frac{1}{2}\sin^2(2\theta).$$

To conclude this comment on orders of magnitude, let us take a look at the detector sizes needed in neutrino experiments. The number of events is given by the product of cross section and integrated luminosity:

$$N_{\text{events}} = \Phi \sigma_{\nu p} T N_p \tag{12.20}$$

where $\Phi \sim 10^{10-12}\,\text{m}^{-2}\text{s}^{-1}$ is the flux of incoming neutrinos, $\sigma_{\nu p} \sim 10^{-45}\,\text{m}^{-2}$ is the cross section[4] of neutrino-proton scattering, $T \sim 1y \simeq 10^7\,\text{s}$ is the observation time and N_p is the number of protons in the target. One can see that, although one can try to increase the flux or measure longer, the main problem is the small cross section $\sigma_{\nu p}$. The only parameter left to tune is the number of protons N_p: To find a reasonable number of events, one has to choose e. g. $N_p > 10^{30}$ which corresponds to about $10^7\,\text{mol}$, i. e. we are talking about detector sizes of tons and kilotons.

Having discussed the behavior of the oscillation term, we can think about what an experiment may be sensitive to. As we have seen, for fast oscillations (large Δm^2) the $\sin^2$ is averaged over and there is, due to uncertainty in E and L no sensitivity on the mass difference (see Fig. 12.3). If the experiment does not find an oscillation signal, one can exclude the RHS region of the curve. To constrain the parameter space, various experiments with different sensibilities are needed.

To attack the case of three light neutrinos, we have to consider a 3×3 mixing matrix. One possible parametrization is ($\Gamma_\delta = \text{diag}(1, 1, e^{i\delta})$)

$$\begin{aligned} U &= O_{23}\Gamma_\delta O_{13}\Gamma_\delta^\dagger O_{12} \\ &= \begin{pmatrix} 1 & 0 & 0 \\ 0 & \cos\theta_{23} & \sin\theta_{23} \\ 0 & -\sin\theta_{23} & \cos\theta_{23} \end{pmatrix} \begin{pmatrix} \cos\theta_{13} & 0 & \sin\theta_{13}e^{-i\delta} \\ 0 & 1 & 0 \\ -\sin\theta_{13}e^{i\delta} & 0 & \cos\theta_{13} \end{pmatrix} \begin{pmatrix} \cos\theta_{12} & \sin\theta_{12} & 0 \\ -\sin\theta_{12} & \cos\theta_{12} & 0 \\ 0 & 0 & 1 \end{pmatrix}. \end{aligned}$$

[4] This is only a rough estimate.

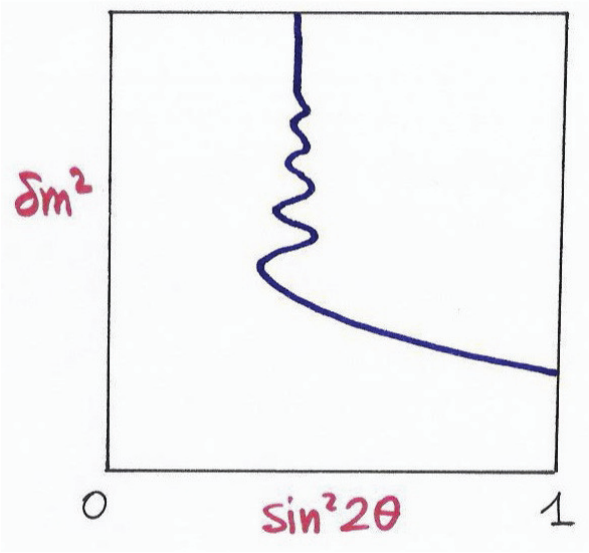

Figure 12.3: *Oscillation experiment sensitivity.* Source: [25].

Experiment shows that $\sin^2\theta_{23} \sim 0.5$ which means almost maximal mixing, $\sin^2\theta_{13} \lesssim$ few %, $\delta = ?$ (small) and $\sin^2\theta_{12} \sim 0.3$. This structure is very different from the CKM case, where the diagonal elements are dominant. What about mass differences in the three-neutrino case? We do not know the absolute ν masses, but they roughly fulfill $m_i \lesssim 1\,\text{eV}$. For ultrarelativistic neutrinos in vacuum we may expand the energy as

$$E = \sqrt{\vec{p}^2 + m_i^2} \simeq |\vec{p}| + \frac{m_i^2}{2E}.$$

Since the oscillation phase is caused by $\Delta E \propto \Delta m_{ij}^2$, this is what oscillation experiments probe. For three neutrinos there are two independent mass differences. For historical reasons the small splitting δm^2 is called "solar" mass^2 splitting:

$$\delta m^2 \simeq 7.7 \cdot 10^{-5}\,\text{eV}^2,$$

for the same reason the large splitting is called "atmospheric" mass^2 splitting:

$$\Delta m^2 \simeq 2.4 \cdot 10^{-3}\,\text{eV}^2.$$

Note that, because $\delta m^2/\Delta m^2 \simeq 1/30$, it is very difficult to be sensitive to both mass splittings in the same experiment (L/E is fixed). The absolute masses m_i are unknown, and thus it is possible to arrange the mass eigenstates in two ways, corresponding to the labeling convention

$$\begin{aligned} \delta m^2 &= m_2^2 - m_1^2 > 0 \\ |\Delta m^2| &= |m_3^2 - m_{1,2}^2| \end{aligned}$$

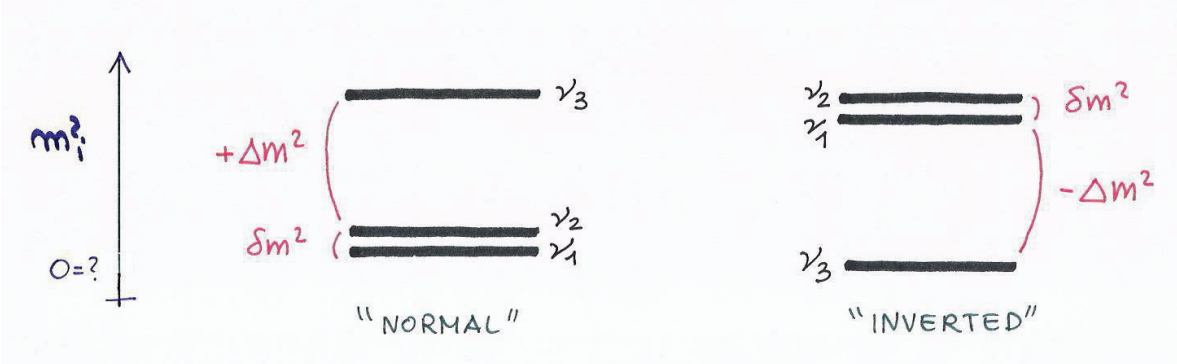

Figure 12.4: *Normal and inverted mass hierarchies for the three-neutrino case.* Source: [25].

(see Fig. 12.4).

To find simple expressions for the oscillation probabilities in the three-neutrino case, we apply two approximations: We neglect the complex phase ($\delta = 0$) and we assume that only one mass scale is relevant:

$$|\delta m^2| \ll |\Delta m^2| \text{ and } |\delta m^2| \ll \frac{E}{L}.$$

This simplified three-neutrino oscillation is described by three parameters only: the mass difference Δm^2, and the mixing angles θ_{13} and θ_{23}. This allows to write the oscillation probabilities as follows [26]:

$$P(\nu_e \to \nu_e) = 1 - \sin^2 2\theta_{13} \sin^2 \frac{\Delta m^2 L}{4E} \tag{12.21}$$

$$P(\nu_e \to \nu_\mu) = \sin^2 2\theta_{13} \sin^2 \theta_{23} \sin^2 \frac{\Delta m^2 L}{4E} \tag{12.22}$$

$$P(\nu_\mu \to \nu_\tau) = \sin^2 2\theta_{13} \sin^2 \theta_{23} \sin^2 \frac{\Delta m^2 L}{4E} \tag{12.23}$$

$$P(\nu_e \to \nu_\tau) = \sin^2 2\theta_{13} \cos^2 \theta_{23} \sin^2 \frac{\Delta m^2 L}{4E} \tag{12.24}$$

$$P(\nu_\mu \to \nu_\tau) = \cos^4 \theta_{13} \sin^2 2\theta_{23} \sin^2 \frac{\Delta m^2 L}{4E}. \tag{12.25}$$

Note that the last equation gives the oscillation probability measured at the OPERA experiment (mentioned above). Not neglecting the CP violating phase δ, one has

$$P(\nu_\alpha \to \nu_\beta) = \delta_{\alpha\beta} - 4 \sum_{i<j} \mathrm{Re} J^{ij}_{\alpha\beta} \sin^2 \left(\frac{\Delta m^2_{ij} L}{4E} \right) - 2 \sum_{i<j} \mathrm{Im} J^{ij}_{\alpha\beta} \sin \left(\frac{\Delta m^2_{ij} L}{2E} \right) \tag{12.26}$$

where $\Delta m_{ij} = m_i^2 - m_j^2$ and $J^{ij}_{\alpha\beta} = U_{\alpha i} U^*_{\beta i} U^*_{\alpha j} U_{\beta j}$. CP violation would be caused by the imaginary part in Eq. (12.26); if it indeed existed, there would be CP violation not only in the quark sector, but also in the lepton sector.

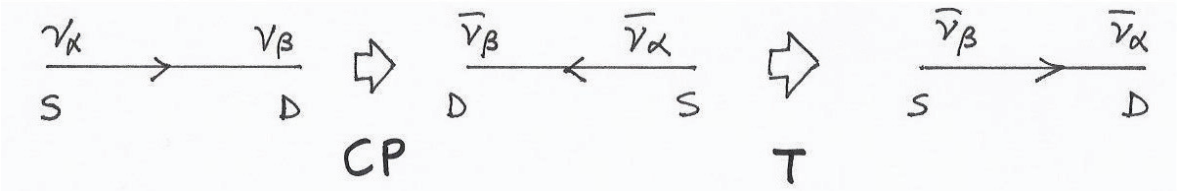

Figure 12.5: *Action of CP and T transformations on the $\nu_\alpha \to \nu_\beta$ process from source (S) to detector (D).* Source: [25].

Let us now take a closer look at the justification of the oscillation probabilities in Eq. (12.21) to (12.25). First consider the influence of symmetries. Figure 12.5 shows the action of CP and T transformations on the $\nu_\alpha \to \nu_\beta$ process from source (S) to detector (D). CP mirrors the setup and trades particles for antiparticles while T reverses the flow of time. This can be summarized as follows:

CP invariance	$P(\nu_\alpha \to \nu_\beta) = P(\bar{\nu}_\alpha \to \bar{\nu}_\beta)$	$(\nu \leftrightarrow \bar{\nu})$
T invariance	$P(\nu_\alpha \to \nu_\beta) = P(\nu_\beta \to \nu_\alpha)$	$(\alpha \leftrightarrow \beta)$
	$P(\bar{\nu}_\alpha \to \bar{\nu}_\beta) = P(\bar{\nu}_\beta \to \bar{\nu}_\alpha)$	
CPT invariance	$P(\nu_\alpha \to \nu_\beta) = P(\bar{\nu}_\beta \to \bar{\nu}_\alpha)$	$(\nu \leftrightarrow \bar{\nu})\&(\alpha \leftrightarrow \beta)$

Looking at Eq. (12.26), one sees that $(\alpha \leftrightarrow \beta)$ or $(\nu \leftrightarrow \bar{\nu})$ amount to $(U \leftrightarrow U^*)$. Therefore, CP invariance requires $U = U^*$, while CPT invariance holds in any case. If the experiments are such that the two approximations used to obtain Eq. (12.21) to (12.25) are valid, the corresponding expressions read

$$P(\nu_\alpha \to \nu_\alpha) = 1 - 4|U_{\alpha 3}|^2(1 - |U_{\alpha 3}|^2)\sin^2\left(\frac{\Delta m^2 L}{4E}\right)$$
$$P(\nu_\alpha \to \nu_\beta) = 4|U_{\alpha 3}|^2|U_{\beta 3}|^2\sin^2\left(\frac{\Delta m^2 L}{4E}\right) \qquad \alpha \neq \beta.$$

Using $|U_{e3}|^2 = \sin^2\theta_{13}$, $|U_{\mu 3}|^2 = \cos^2\theta_{13}\sin^2\theta_{23}$, $|U_{\tau 3}|^2 = \cos^2\theta_{13}\cos^2\theta_{23}$, one recovers Eq. (12.21) to (12.25). Measurements based on these results are neither sensitive to the type of mass hierarchy nor to CP violation. Also there is no sensitivity to δm^2 and θ_{12}. Finally, there is no difference between the expressions for ν and $\bar{\nu}$. Table 12.1 shows a summary of the experiments for which the said approximation, $\Delta m^2 L/(4E) \simeq 1$, holds. These include atmospheric neutrino experiments (ATM), long-baseline accelerator experiments (LBL) and short-baseline reactor experiments (SBR). Note that the first two oscillation probabilities reduce to the two-neutrino form for $\theta_{13} \to 0$ and the second two are constant for $\theta_{13} \to 0$.

At the other side of the mass spectrum, there are experiments mainly sensitive to δm^2

Experiment	Measurement
OPERA (LBL)	$P(\nu_\mu \to \nu_\tau) \simeq \mathrm{c}_{13}^4 \sin^2 2\theta_{23} \sin^2(\Delta m^2 L/(4E))$
K2K, MINOS (LBL), atmospheric	$P(\nu_\mu \to \nu_\mu) \simeq 1 - 4\mathrm{c}_{13}^2\mathrm{s}_{23}^2(1 - \mathrm{c}_{13}^2\mathrm{s}_{23}^2) \sin^2(\Delta m^2 L/(4E))$
ATM, LBL	$P(\nu_\mu \to \nu_e) \simeq \mathrm{s}_{23}^2 \sin^2 2\theta_{13} \sin^2(\Delta m^2 L/(4E))$
CHOOZ (SRB)	$P(\nu_e \to \nu_e) \simeq 1 - \sin^2 2\theta_{13} \sin^2(\Delta m^2 L/(4E))$

Table 12.1: *Summary of neutrino experiments with* $\Delta m^2 L/(4E) \simeq \infty$. $\mathrm{s}_{ij}^2 = \sin^2\theta_{ij}$ and $\mathrm{c}_{ij}^2 = \cos^2\theta_{ij}$.

where

$$\frac{\delta m^2 L}{4E} \simeq \mathcal{O}(1) \tag{12.27}$$

$$\frac{\Delta m^2 L}{4E} \gg 1. \tag{12.28}$$

In this case

$$P(\nu_e \to \nu_e) \simeq \cos^4\theta_{13}\left[1 - \sin^2 2\theta_{12} \sin^2\left(\frac{\delta m^2 L}{4E}\right)\right] + \sin^4\theta_{13} \tag{12.29}$$

which holds e. g. for the KamLAND long-baseline reactor experiments. Note that also in this case there is no dependence on hierarchy, neutrino-antineutrino interchange and CP violation.

To conclude the theory part, let us summarize the above discussion. We have worked out approximate oscillation probabilities as a function of dominant mass mixing parameters for different classes of experiments (see Fig. 12.6). Furthermore, we have seen that the smallness of θ_{13} and of $\delta m^2/\Delta m^2$ make it difficult to probe CP violation and the hierarchy via oscillations in current experiments. Finally [27, p. 215], matter effects can occur if the neutrinos under consideration experience different interactions by passing through matter. In the Sun and the Earth ν_e can have neutral-current and charged-current interactions with leptons because of the existence of electrons, while for ν_μ and ν_τ only neutral-current interactions are possible. This is not being discussed any further here, see e. g. [27].

12.4.2 Phenomenology – experiments and current knowledge

Figure 12.7 shows combined results of neutrino experiments. In the excluded regions, no oscillations are observed; note that the (more or less) symmetric shape in the upper part of the plot is because for the three-neutrino case (and because of matter effects) the dependence is not only on $\sin^2 2\theta$, such that octant symmetry, $P(\theta) = P(\pi/2 - \theta)$, (see also Fig. 12.3) does not hold in general and the second octant has to be unfolded (see Fig. 12.8). In any case, one realizes that there are many experimental results available.

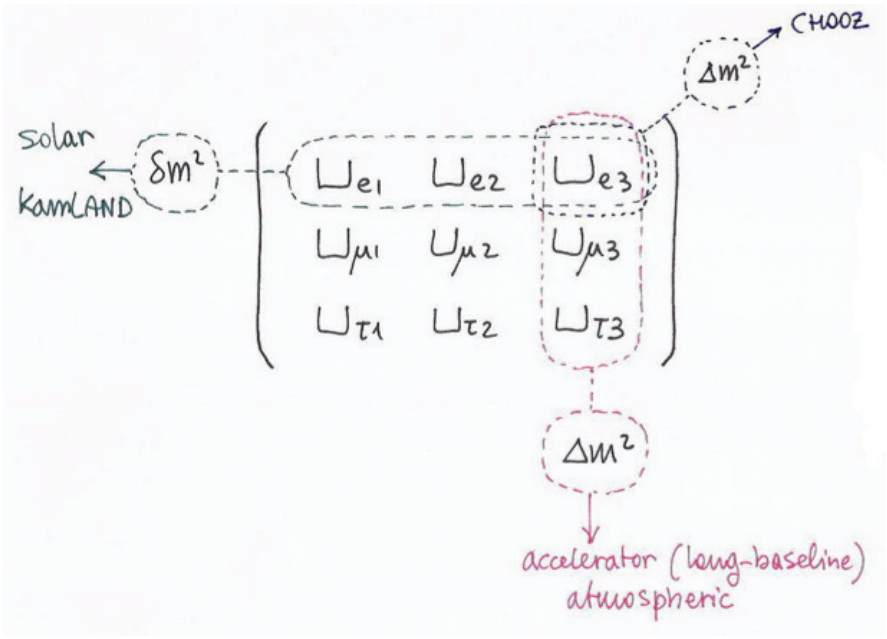

Figure 12.6: *Summary of experimental sensitivities to the neutrino mixing matrix.* Source: [25].

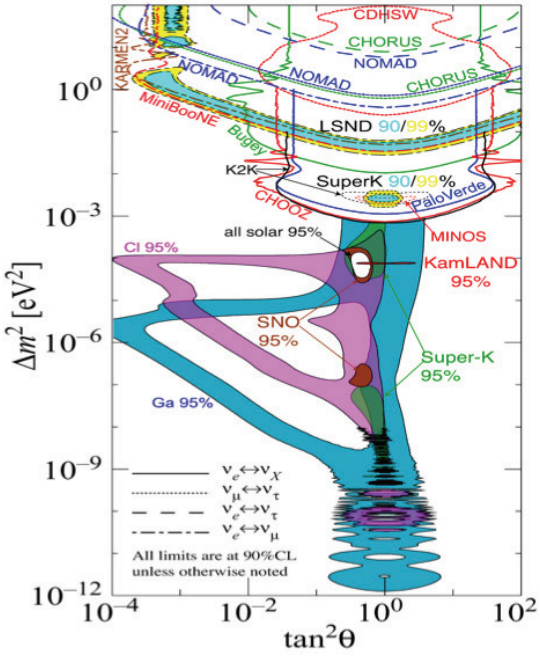

Figure 12.7: *Summary of neutrino oscillation experiments.* Source: Particle Data Group 2009.

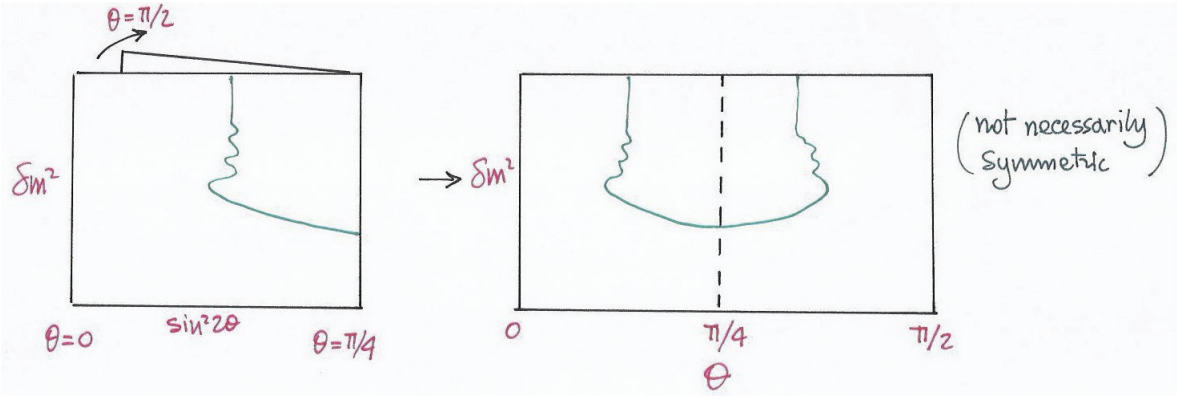

Figure 12.8: *Oscillation experiment sensitivity as a function of* θ*, rather than* $\sin^2 2\theta$. Source: [25].

Their three-neutrino interpretation is summarized in Fig. 12.9; the numerical values (with one digit accuracy) read:

$$\begin{aligned} \delta m^2 &\sim 8 \cdot 10^{-5}\,\mathrm{eV}^2 \\ \Delta m^2 &\sim 3 \cdot 10^{-3}\,\mathrm{eV}^2 \\ m_\nu &< \mathcal{O}(1)\,\mathrm{eV} \\ \mathrm{sign}(\Delta m^2) &= ? \\ \sin^2\theta_{12} &\sim 0.3 \\ \sin^2\theta_{23} &\sim 0.5 \\ \sin^2\theta_{13} &\sim \text{few}\,\% \\ \delta(CP) &= ?. \end{aligned}$$

Figure 12.10 gives an overview of which type of experiment contributed to the individual parts of the present knowledge on neutrino mass properties. In the following we discuss how such information is constrained by the following types of experiments:

- Short-baseline reactor;
- Atmospheric;
- Long-baseline accelerator and
- Solar.

The short-baseline reactor experiment CHOOZ. Figure 12.11 shows the general setup of the CHOOZ experiment. Nuclear fission in a reactor produces antineutrinos via neutron decay: $n \to p + e^- + \bar{\nu}_e$, leading to production rates as high as $\sim 6 \cdot 10^{20}\,\mathrm{s}^{-1}$, the

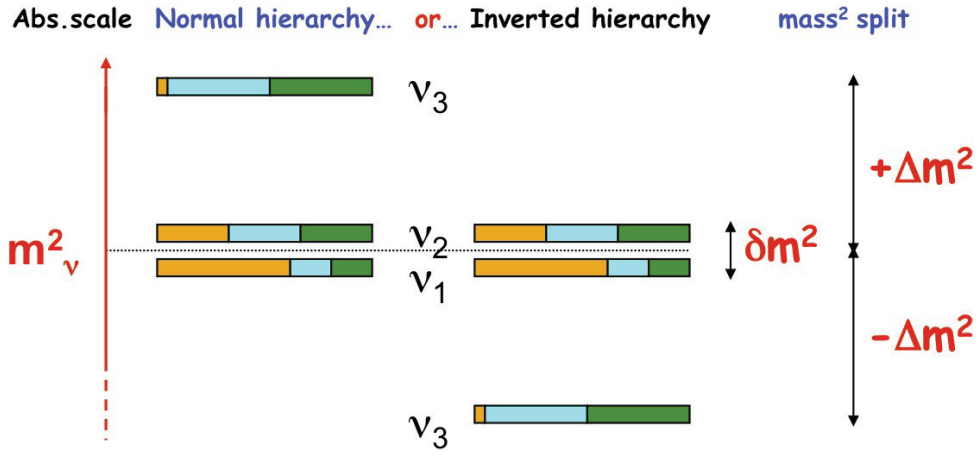

Figure 12.9: *Summary of the current knowledge on neutrino oscillations.* Source: [25].

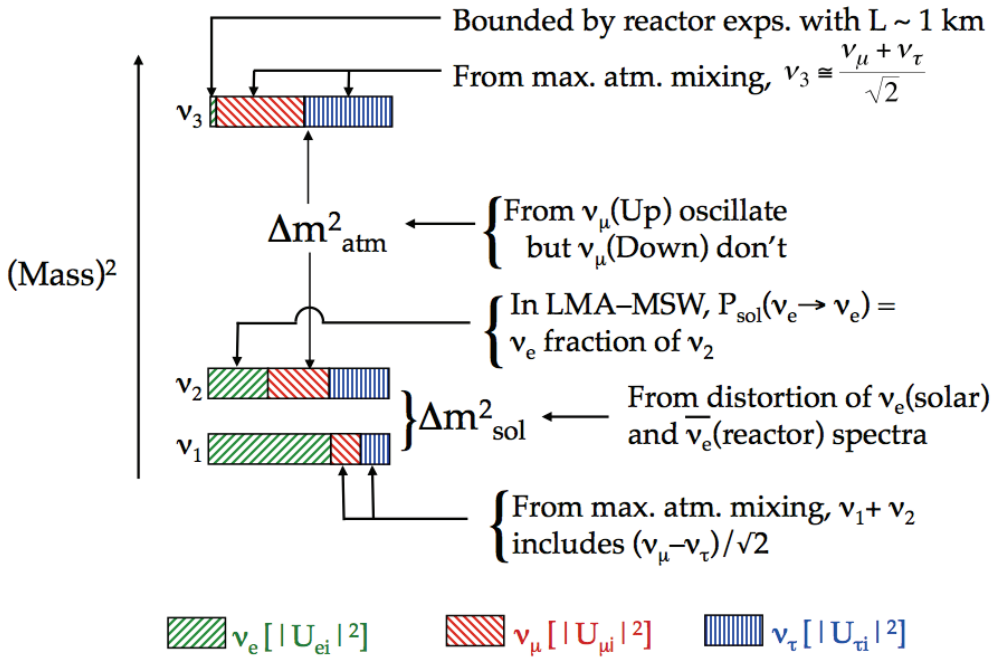

Figure 12.10: *Origin of the current knowledge on neutrino oscillations.* Source: B. Kayser.

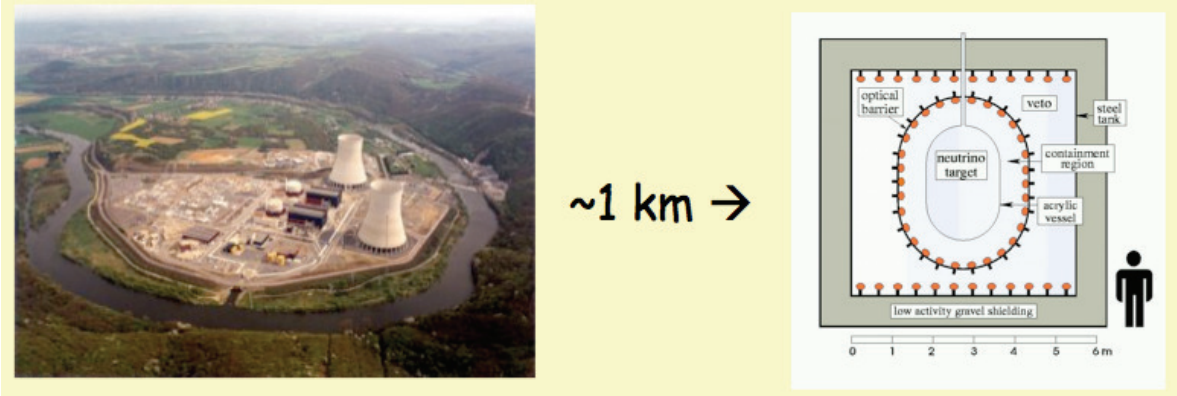

Figure 12.11: *Setup of short-baseline reactor experiments.* Source: [25].

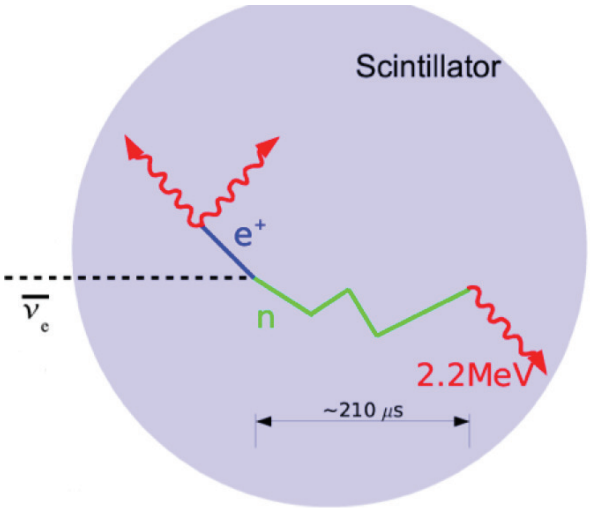

Figure 12.12: *Neutrino detection via inverse beta decay.*

energy being of the order of MeV. Detection is accomplished by inverse β-decay: $\bar{\nu}_e + p \rightarrow e^+ + n$; $n + p \rightarrow d + \gamma$, i. e. an incoming antineutrino hits a proton in the scintillator which acts both as target and detector, producing a positron and a neutron (see Fig. 12.12). In the scintillator, the positron annihilates with an electron to produce two photons, both at 511 keV. Some 210 μs later the neutron is captured, producing an excited state, which decays emitting a photon of about 2.2 MeV. Taken together, due to their energy and temporal pattern, the three photons produced in total constitute a clear signature. In particular, the fact that the third γ is delayed allows for good background rejection. What does one expect assuming that there are no oscillations visible with this setup? The reactor antineutrino spectrum is shown in Fig. 12.13(a) together with the cross section for inverse β-decay. Convoluting both distributions yields the observed spectrum. However, if there are oscillations the picture changes (see Fig. 12.13(b)). As one can see in Fig. 12.13(c), the CHOOZ results are in agreement (within a few % error) with the assumption that there are no oscillations happening. Based on the one-mass scale dominance interpretation discussed above, one uses the disappearance formula in Tab. 12.1 to produce the exclusion plot shown in Fig. 12.13(d). To reduce systematics (by using a second close detector), there is worldwide activity to build a new reactor experiment with higher θ_{13} resolution.

Atmospheric neutrinos: the Super-Kamiokande breakthrough. Figure 12.14(a) shows the zenith angle dependence of the number of events in the 50 kt Super-Kamiokande detector. One observes that there is a deficit in μ-like events in the up-going direction, whereas the electron-like events follow more or less the expectations. Atmospheric neutrinos with electron or muon flavor are produced as secondary (anti)particles in decays of mesons produced by cosmic rays hitting the atmosphere (see Fig. 12.15(b)). Although the primary flux is affected by large normalization uncertainties, the neutrino flavor ratio (about twice as much μ neutrinos than electron-neutrinos) is robust within a few per-cent. As we have seen, the idea is to look up and down, since the neutrino flux from opposite directions is the same, because for the opposite side the increased flux dilution ($\sim 1/r^2$) is compensated by the larger production surface ($\sim r^2$) (see Fig. 12.14(b)). The actual detection employs again charged-current interactions in the target. It is possible to distinguish the muonic from the electronic final state by means of the Cherenkov ring sharpness: Producing showers in the target, the electron/positron smears out its Cherenkov ring (see Fig. 12.16). This method does not allow for charge discrimination and τ events are not reconstructed. A summary of the zenith distributions at Super-Kamiokande is shown in Fig. 12.17. One can observe that the distribution of electronic events is more or less in agreement with the expectation for no mixing, while there is a deficit in muonic events from below, compared to the expectation for no oscillation. Observations over several decades of L/E show the same results. How to interpret them? In terms of oscillations this means that the channel $\nu_\mu \rightarrow \nu_e$ is non-existing or subdominant (in agreement with CHOOZ) and that the channel $\nu_\mu \rightarrow \nu_\tau$ is dominant. Recall that the one-mass scale

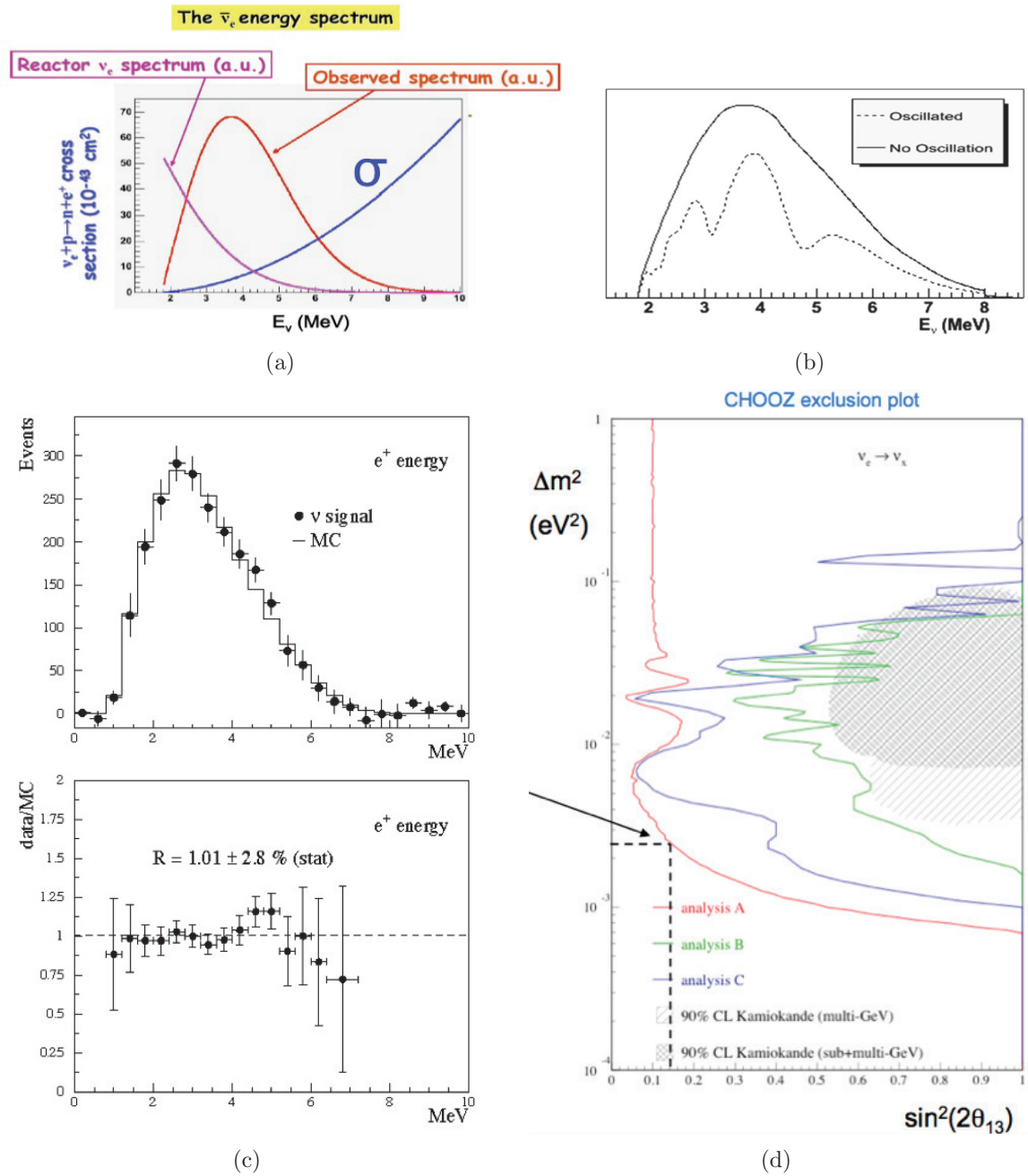

Figure 12.13: *Results of the short-baseline reactor experiment CHOOZ.*

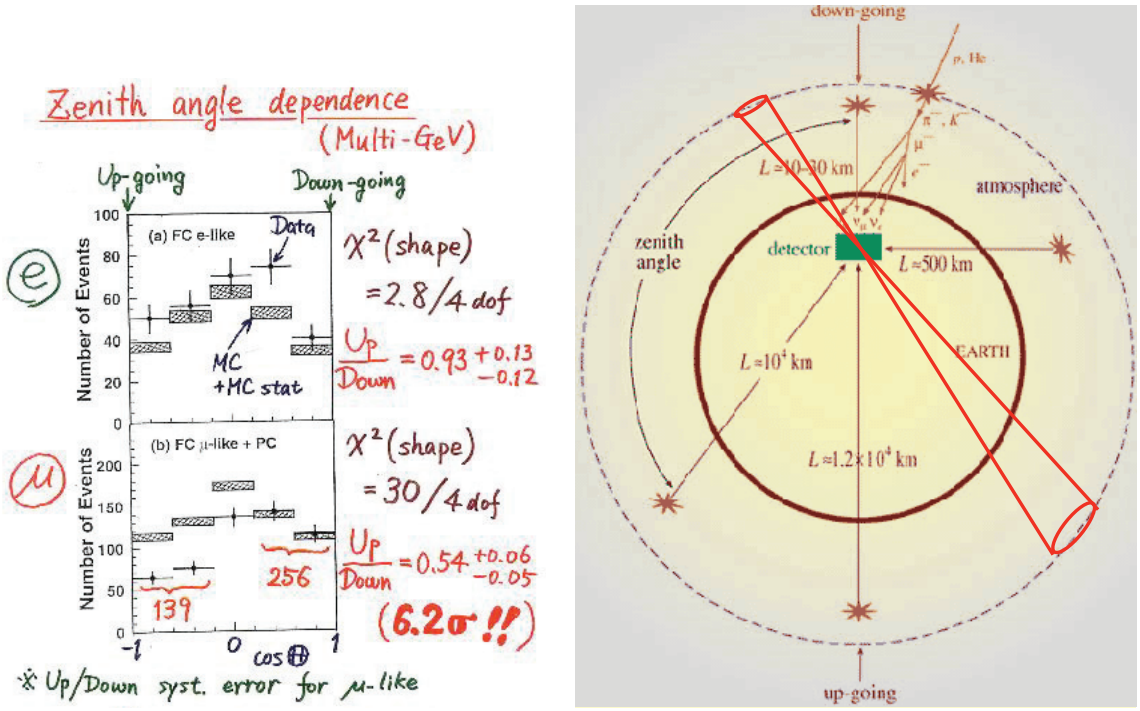

(a) (b)

Figure 12.14: *Zenith angle dependence of μ-like events in the Super-Kamiokande experiment.* Source: T. Kajita at Neutrino '98, Takayama.

approximation for $\theta_{13} = 0$ reads

$$P(\nu_\mu \to \nu_\tau) = \sin^2 2\theta_{23} \sin^2 \left(\frac{\Delta m^2 L}{4E} \right) . \tag{12.30}$$

The results are consistent with other atmospheric experiments using different techniques (MACRO, Soudan2) but with lower statistics. Performing a dedicated L/E analysis in Super-Kamiokande, it is even possible to "see" one half-period of the oscillation (distorted by convolution with resolution, see Fig. 12.18(a)). Overall, the Super-Kamiokande measurement yields strong constraints on the parameters Δm^2 and θ_{23} (see Fig. 12.18(b)).

Long-baseline neutrino experiments. With long-baseline experiments it is possible to reproduce atmospheric μ-neutrino physics under controlled conditions (known flux etc.). Sketches of such experiments in the US, Japan and Europe are shown in Fig. 12.19. An example of neutrino beam production is shown in Fig. 12.20. Protons hitting a fixed target produce pions which in turn decay into muons and muon neutrinos. To obtain a focussed beam, the pions have to be focussed in the first place. This is achieved with magnetic lenses, so called "horns". Due to the production mode via pion decay, there is a small contamination by electron neutrinos. Far detection of the neutrinos is achieved by

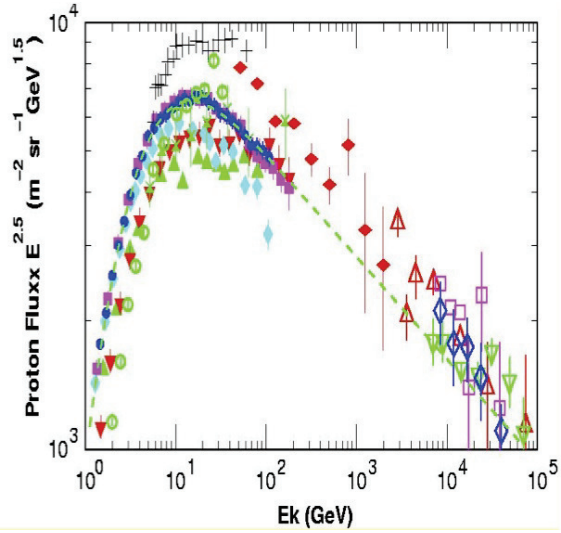

(a) (b)

Figure 12.15: *Production of atmospheric neutrinos.* The absolute value of the primary flux is not known precisely (a), but the flavor ratio is robust within a few percent (b).

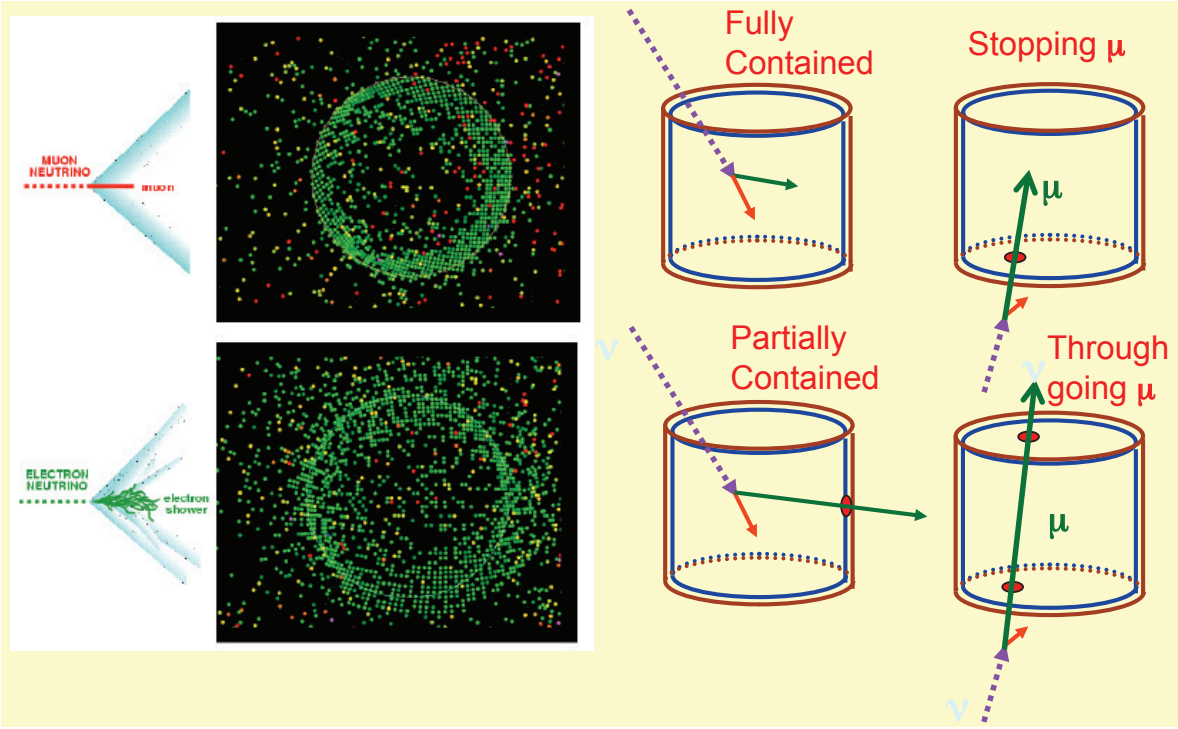

Figure 12.16: *Detection in Super-Kamiokande.* Parent neutrinos are detected via charged-current interactions in the water target.

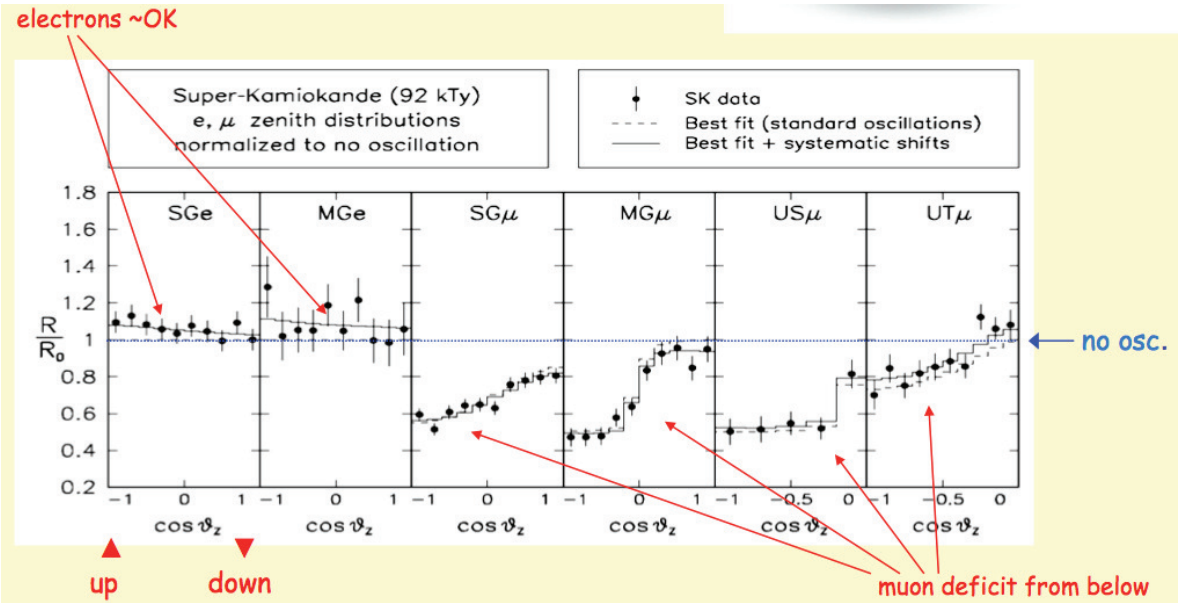

Figure 12.17: *Super-Kamiokande results on atmospheric neutrinos.*

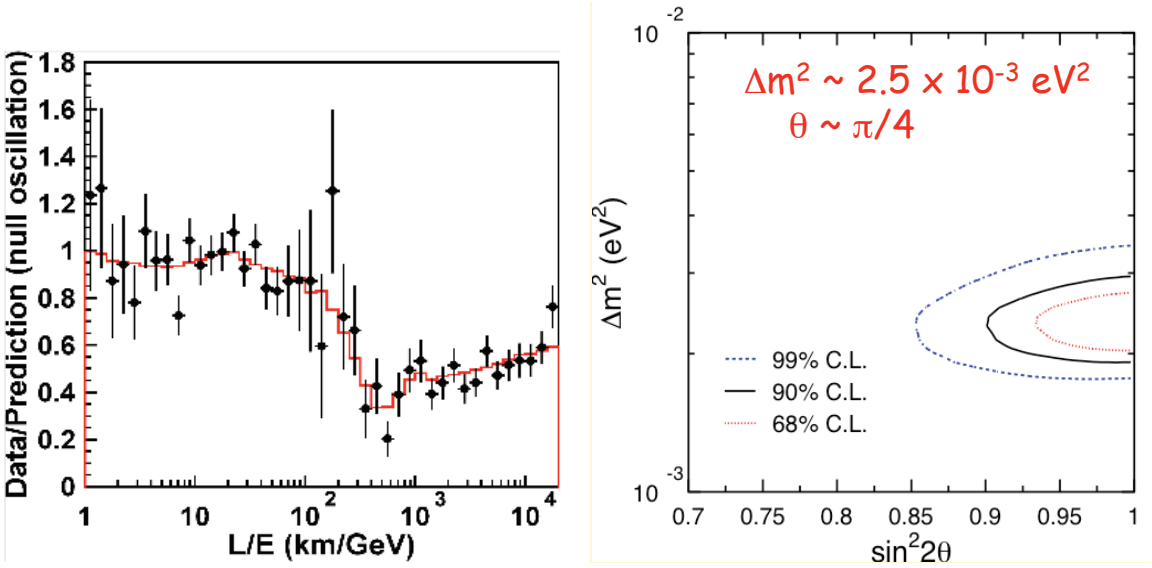

(a) (b)

Figure 12.18: *Super-Kamiokande results on oscillation period (a) and constraints on the parameters Δm^2 and θ.*

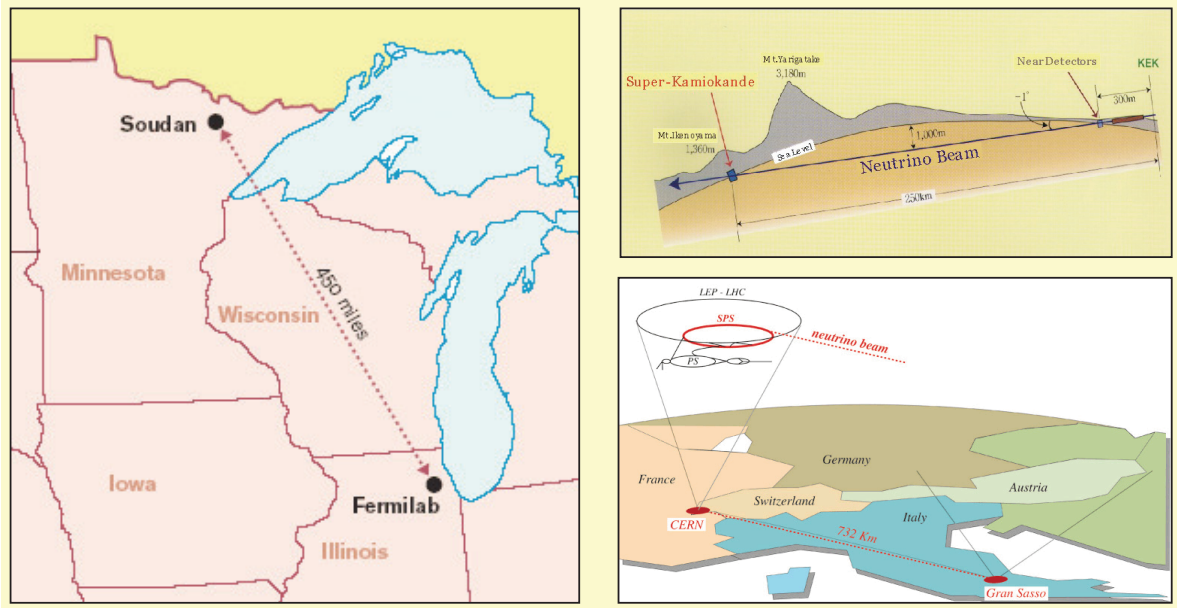

Figure 12.19: *Examples of long-baseline neutrino experiments.* Source: [25].

the Cherenkov technique at Super-Kamiokande (K2K and T2K) or by a steel/scintillator detector in the case of MINOS. Both experiments are supplemented by near detectors to control the flux of muon neutrinos for normalization. Once more the dominant probability is $P(\nu_\mu \to \nu_\tau) = \sin^2 2\theta_{23} \sin^2(\Delta m^2 L/4E)$ such that the results can be compared to the atmospheric results. Combining the corresponding exclusion plots, one finds the oscillation parameters to be consistent among the experiments (see Fig. 12.21). The OPERA detector searches for dominant oscillations via τ appearance. This is done using a hybrid of emulsion layers and scintillator trackers: If the tracker indicates a candidate event, the layers are scanned to document tau decays (see Fig. 12.22).

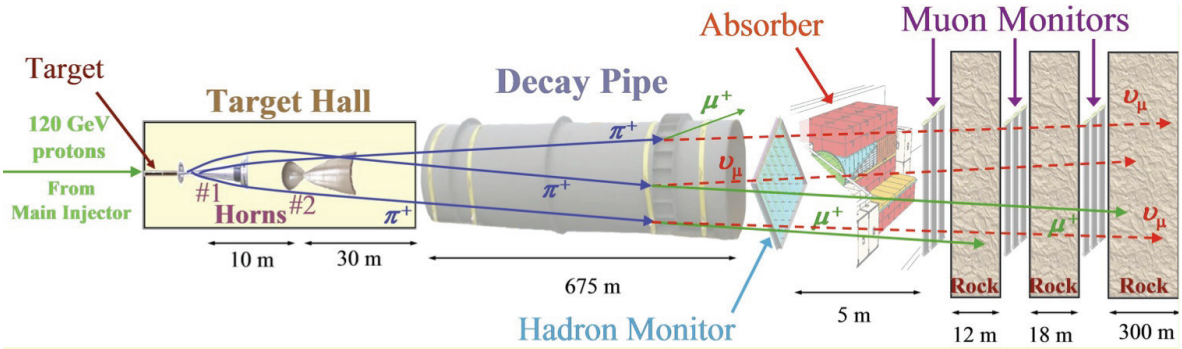

Figure 12.20: *Muon-neutrino beam production at hadron accelerators.*

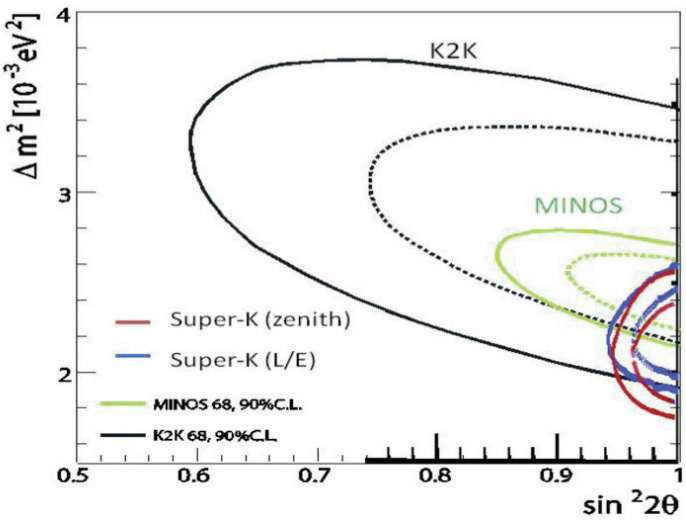

Figure 12.21: *Long-baseline neutrino experiments combination and consistency check with atmospheric results.*

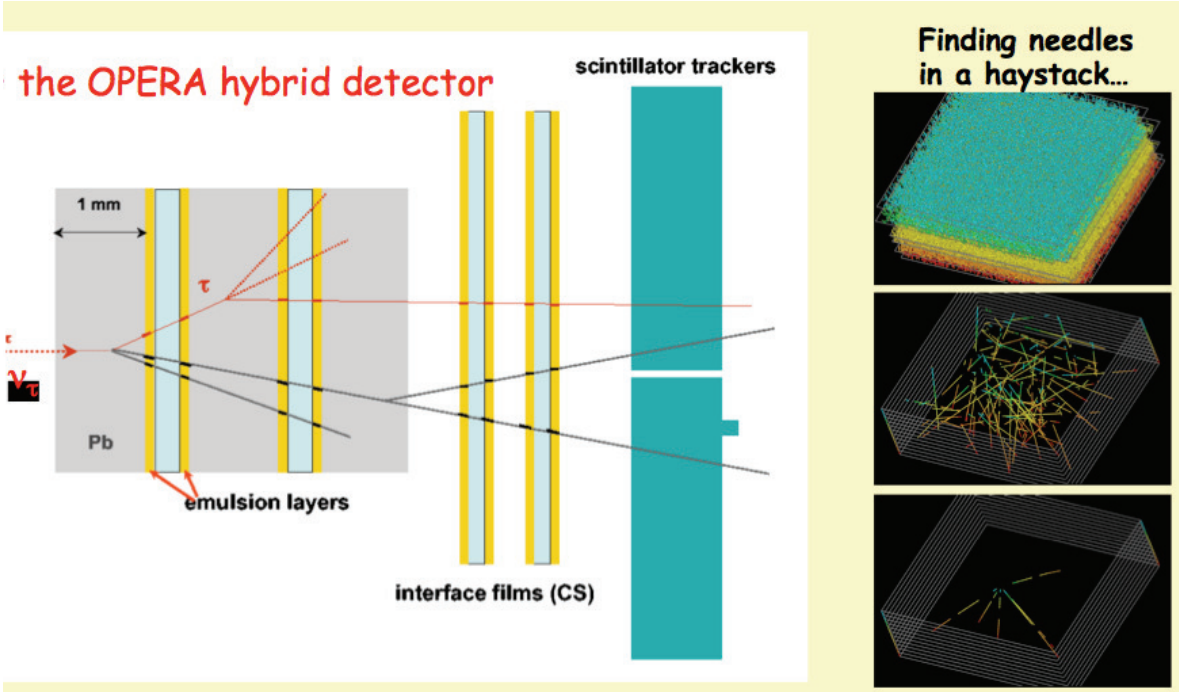

Figure 12.22: *Sketch of the OPERA detector (LHS) and of a reconstructed event (RHS).*

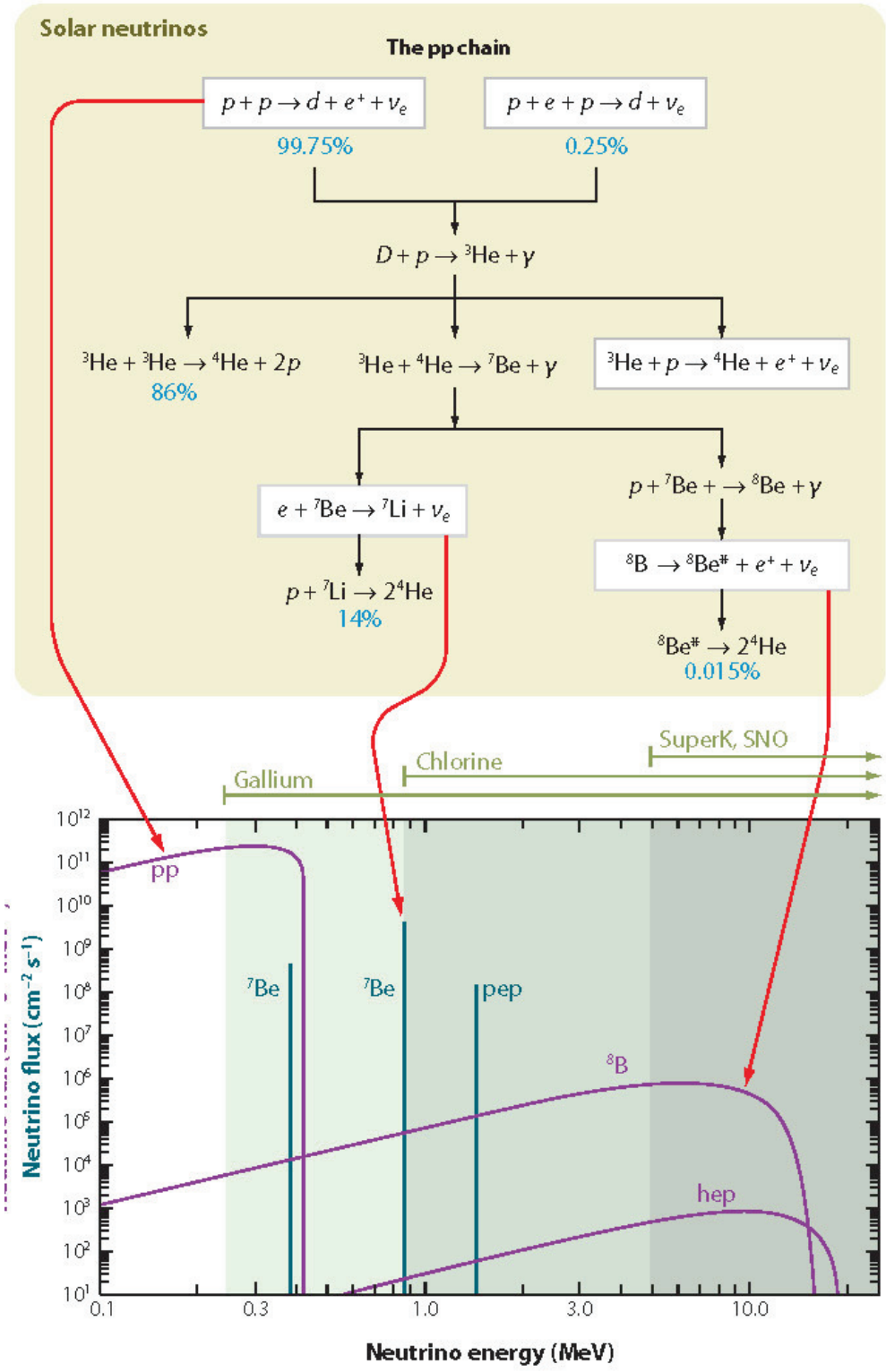

Figure 12.23: *Production of solar neutrinos in the pp cycle.*

Solar neutrinos. We now turn to experiments sensitive to the small mass splitting δm^2. Solar neutrino production proceeds via the *pp* (and CNO) cycles (see Fig. 12.23), where the energy spectrum of the neutrinos varies with the stage of their production. There are different ways to detect "solar neutrinos". In the radiochemical method, one counts the decays of unstable final-state nuclei. Advantageous is the low energy threshold of this method. Problematic is, though, the loss/integration of the energy and time information. Possible reactions for detection are

$$\begin{array}{lll} {}^{37}\mathrm{Cl} + \nu_e \to {}^{37}\mathrm{Ar} + e^- & \text{(CC)} & \text{Homestake} \\ {}^{71}\mathrm{Ga} + \nu_e \to {}^{71}\mathrm{Ge} + e^- & \text{(CC)} & \text{GALLEX/GNO, SAGE.} \end{array}$$

The second detection possibility for solar neutrinos is elastic scattering:

$$\nu_x + e^- \to \nu_x + e^- \qquad \text{(NC,CC)} \qquad \text{SK, SNO, Borexino}$$

where events are detected in real time with either a high energy threshold (Cherenkov, directional) or with a low threshold (scintillators). Thirdly, there is the possibility to detect solar neutrinos via interactions with deuterium, where the charged current events are detected in real time and the neutral current events are separated statistically and using neutron counters. The corresponding reactions read:

$$\begin{array}{lll} \nu_e + \mathrm{d} \to p + p + e^- & \text{(CC)} & \text{SNO} \\ \nu_x + \mathrm{d} \to p + n + \nu_x & \text{(NC)} & \text{(Sudbury Neutrino Observatory).} \end{array}$$

All CC-sensitive results on solar neutrinos indicated a ν_e deficit, when compared to solar model expectations (see Fig. 12.24(a)). Interpreting the results in terms of neutrino oscillations yielded solar constraints on δm^2 and θ_{12} (see Fig. 12.24(b)). A crucial role in this development was played by the Sudbury Neutrino Observatory. As we have seen, at SNO deuterium was used as target. In deuterium one can separate CC events (induced by ν_e only) from NC events (induced by $\nu_e,\ \nu_\mu,\ \nu_\tau$), and double check via elastic scattering events (due both to NC and CC). In terms of flux this means

$$\frac{\mathrm{CC}}{\mathrm{NC}} \simeq \frac{\Phi(\nu_e)}{\Phi(\nu_e) + \Phi(\nu_{\mu,\tau})}.$$

Therefore

$$\frac{\mathrm{CC}}{\mathrm{NC}} < 1 \Rightarrow \Phi(\nu_{\mu,\tau}) > 0 \Rightarrow P(\nu_e \to \nu_{\mu,\tau}) \neq 0$$

since solar neutrinos are produced exclusively as electron neutrinos. It was found that $\mathrm{CC/NC} \sim 1/3 < 1$ and the solar model turned out to be adequate. Note also that since $\mathrm{CC/NC} \sim P(\nu_e \to \nu_e) \sim 1/3 < 1/2$ this is also evidence of three-neutrino like mixing and of matter effects. A summary of neutrino mass differences and mixing parameters with their $n\sigma$ ranges from a global three-neutrino analysis is shown in Fig. 12.25.

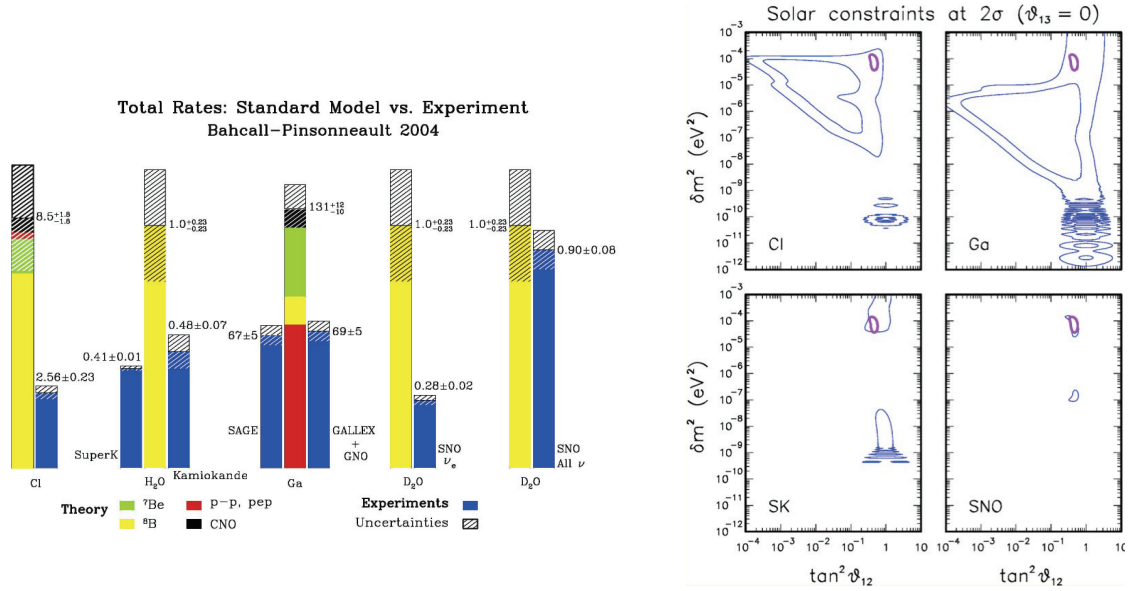

(a) (b)

Figure 12.24: *Electron neutrino deficit in solar neutrino measurements as compared to standard solar model (a) and parameter constraints from interpretation in terms of mixing (b).*

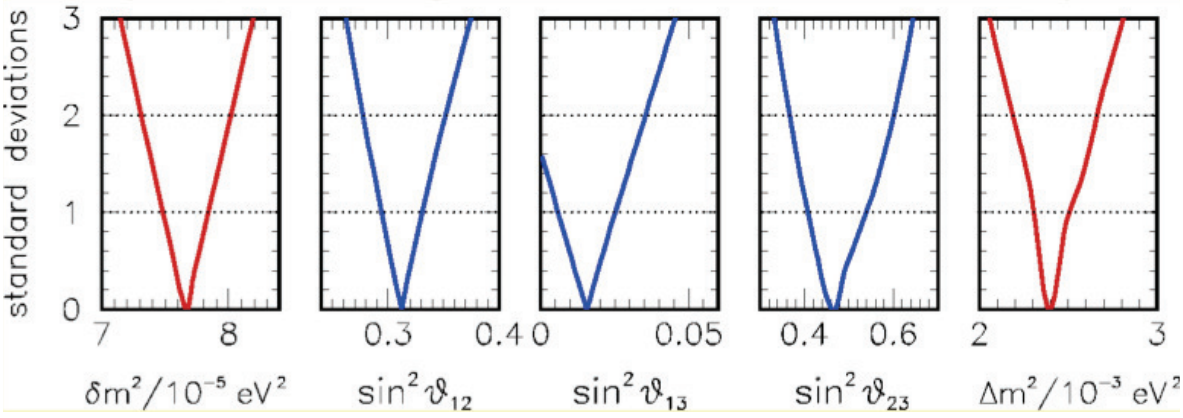

Figure 12.25: *Synopsis of neutrino mass splitting and mixing parameters.*

What are the next experimental steps in determining these parameters? First of all it is important to know θ_{13} more precisely. Since $\sin^2\theta_{13} = |U_{e3}|^2$, this is the small ν_e part of ν_3. Thus what is needed is an experiment with L/E sensitive to Δm ($L/E \sim 500\,\mathrm{km/GeV}$), and involving ν_e. One possibility is disappearance of $\bar{\nu}_e$ produced by a reactor while traveling $L \sim 1.5\,\mathrm{km}$. This process depends on θ_{13} alone (recall Eq. (12.21)):

$$P(\bar{\nu}_e \text{ disappearance}) = \sin^2 2\theta_{13} \sin^2 \frac{\Delta m^2 L}{4E}.$$

Another interesting possibility is the measurement of $P(\nu_\mu \to \nu_e)$ for ν_μ produced by accelerators with L several hundred kilometers. This process depends on θ_{13}, θ_{23}, on whether the hierarchy is normal or inverted and on whether CP is violated (δ).

12.4.3 Absolute masses

As we have seen, neutrino oscillations constrain neutrino mixings and mass splittings but not the absolute mass scale. E. g., one can choose the lightest neutrino mass as a free parameter. However, the lightest neutrino mass cannot be directly observed. There are three realistic observables to attack neutrino masses:

1. β decay. A non-vanishing neutrino mass can affect the spectrum endpoint in β decay.
2. Neutrinoless double beta decay. This is only possible for Majorana neutrinos, we will not discuss this possibility here.
3. Cosmology. Non-vanishing neutrino masses can affect large scale structures in the standard model of cosmology, constrained by CMB and other data. Again, we will not go into detail here.

One can use the high energy end of a beta decay spectrum like the one shown in Fig. 11.1(a) to search for neutrino masses. Since beta decay is essentially emission and decay of a W boson, the matrix element squared is proportional to G_F^2. Thus the decay rate reads $d\Gamma \propto G_F^2 \times$ (phase space factor). The energy spectrum can be written as

$$\frac{d\Gamma}{dE_e} \propto \begin{cases} G_F^2 p_e E_e (Q - E_e)^2 & (m_\nu = 0) \\ G_F^2 p_e E_e (Q - E_e)\sqrt{(Q - E_e)^2 + m_\nu^2} & (m_\nu > 0) \end{cases}$$

where Q is the high energy endpoint of the electron spectrum. Tritium is well suited for this experiment, since Q (18.57 keV) and half life (12.32 y) are low. The reaction reads as follows:

$$^3\mathrm{H} \to {}^3\mathrm{He} + e^- + \bar{\nu}_e.$$

Figure 12.26 shows a close-up of the spectrum around its endpoint. Note that only a very small fraction of all events lies in the region sensitive to the neutrino mass. To detect its

effect, good energy resolution is needed. In fact, E_0 is not Q, but the end point value corrected by a recoil contribution which can be assumed to be constant in the region of interest ($E_{\mathrm{rec}} = 1.72\,\mathrm{eV}$): $E_0 = Q - E_{\mathrm{rec}}$ (see [28, 29] for details).

There are three mass eigenstates whose eigenvalues cannot be individually resolved by this experiment: Beta-decay produces electron neutrinos; as we have seen, these are superpositions of the three mass eigenstates ν_i. Therefore, the experiment is sensitive to the sum of the masses m_i, weighted by the squared mixing coefficients $|U_{ei}|^2$:

$$m_\beta = \sqrt{\mathrm{c}_{13}^2\mathrm{c}_{12}^2 m_1^2 + \mathrm{c}_{13}^2\mathrm{s}_{12}^2 m_2^2 + \mathrm{s}_{13}^2 m_3^2}$$

which is called "effective electron neutrino mass". Note that the mass eigenstate with the largest electron flavor component is ν_1, $|U_{e1}|^2 \simeq \cos^2\theta_{12} \simeq 0.7$, and it cannot be excluded that ν_1 is nearly massless (in the normal hierarchy, see Fig. 12.4). A historical summary of the mass limits obtained by the beta-decay method is shown in Fig. 12.27. Latest bounds are at the level of 2 eV.

The significant improvement in the neutrino mass sensitivity at the Troitsk and the Mainz experiments (compared to the older ones) is due to so-called MAC-E-Filters (Magnetic Adiabatic Collimation with an Electrostatic Filter) [28, p. 17]. Figure 12.28 shows the main features of the MAC-E-Filter. β electrons emitted by the tritium source in the LHS solenoid into the forward hemisphere are guided magnetically on a cyclotron motion along the magnetic field lines into the spectrometer, resulting in an accepted solid angle of nearly 2π. On their way into the center of the spectrometer the magnetic field B drops adiabatically by several orders of magnitude keeping the ratio of cyclotron energy and magnetic field constant: $E_\perp/B = \mathrm{const}$. Therefore, nearly all cyclotron energy $E_\perp$ is transformed into longitudinal motion giving rise to a broad beam of electrons flying almost parallel to the magnetic field lines. Finally, the parallel beam of electrons is energetically analyzed by applying an electrostatic barrier. The KATRIN experiment, currently under construction, is expected to improve the mass limit by one order of magnitude to about 0.2 eV.

Neutrino physics is a vast field, accordingly important topics like Majorana neutrinos, neutrino-less double-beta decay, cosmological bounds on the neutrino mass and future perspectives in neutrino physics are not discussed here (see lecture on neutrino physics by Prof. Rubbia[5]).

[5] http://neutrino.ethz.ch/Vorlesung/HS2009/

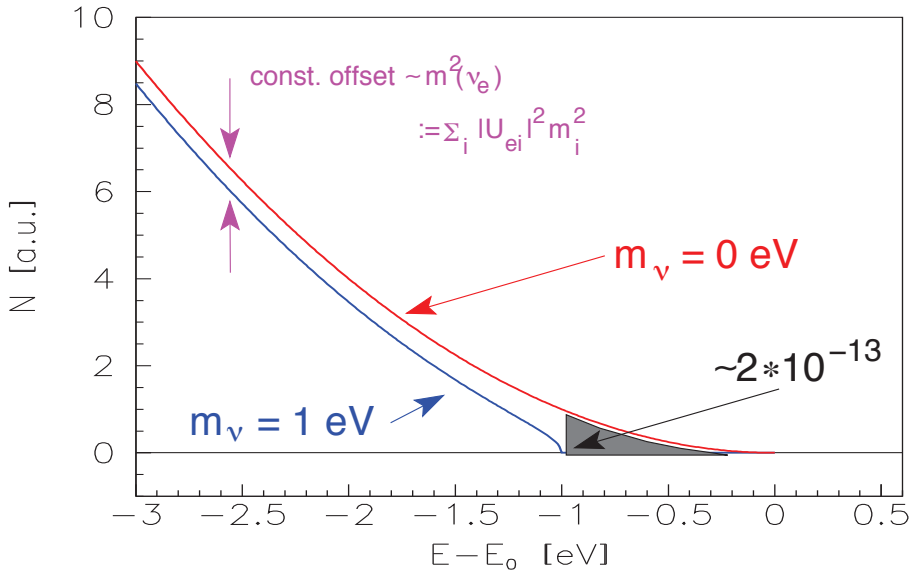

Figure 12.26: *Close-up of the high-energy end of the beta decay spectrum.* In the case of tritium the shaded area corresponds to a fraction of about $2 \cdot 10^{-13}$ events. Source: [28, p. 12].

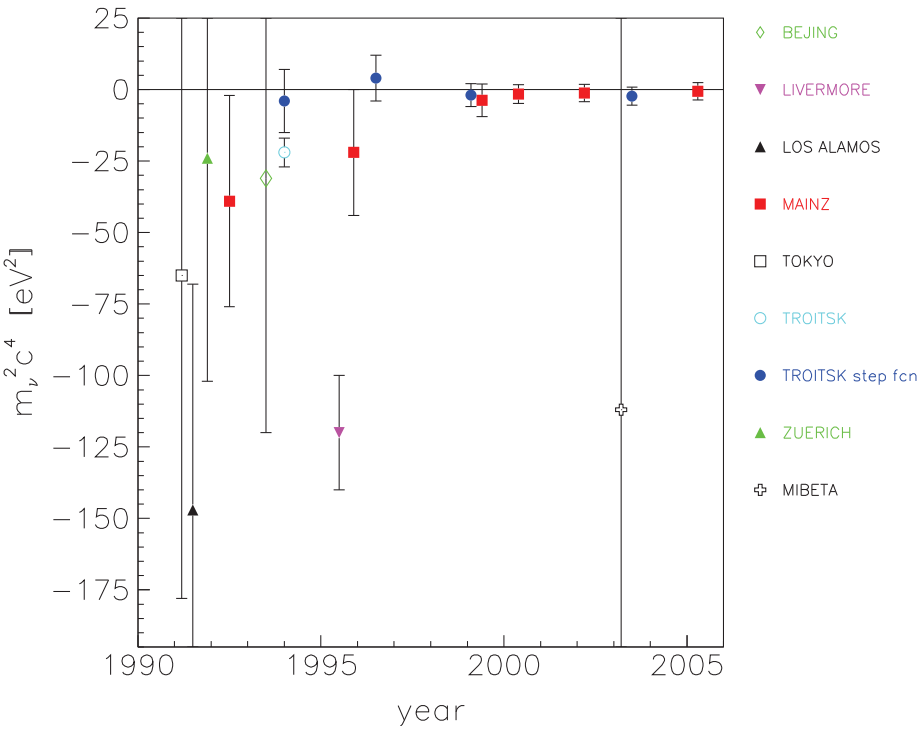

Figure 12.27: *Recent results of tritium beta decay experiments on the effective electron neutrino mass.* Source: [28, p. 15].

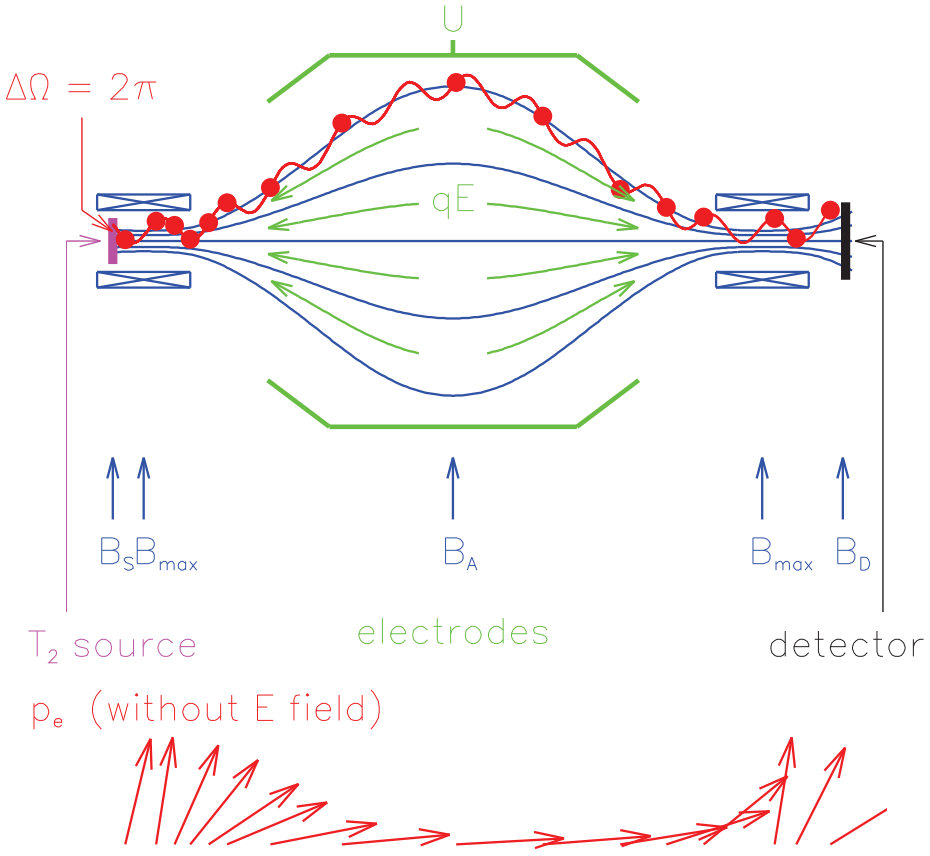

Figure 12.28: *Sketch of the MAK-E-Filter.* Source: [28, p. 17].